Effects of Tidal Range on Mooring Systems of Wave Energy Converters

Stephen Murphy[1], Majid A. Bhinder[2], Pierre Casaubieilh[3], Wanan Sheng[4]
MaREI
University College Cork, Ireland
[1]108422613@umail.ucc.ie, [2]mbhinder@ucc.ie, [3]p.casaubieilh@ucc.ie, [4]W.Sheng@ucc.ie

I. KEYWORDS

Mooring, Wave Energy Converters, Tidal Range, ANSYS AQWA, Galway Bay

II. ABSTRACT

Wave energy converters are currently proposed to be deployed near coastal area for the closeness to the infrastructure and for ease of maintenance in order to reduced operational costs. The motivation behind this work is the fact that the deployment depths during the highest and lowest tides will have a significant effect on the mooring system of WECs. In this paper, the issue will be investigated by numerical modelling (using ANSYS AQWA) for both catenary and taut moorings to examine the performance of the mooring system in varying tides. The case study being considered is the ¼- scale wave energy test site in Galway Bay off the west coast of Ireland where some marine renewable energy devices can be tested. In this test site, the tidal range is macro-tidal with a range of approximately 6 m which is a large value relative to the water depth. In the numerical analysis, ANSYS AQWA suite has been used to simulate moored devices under wave excitation at varying tidal ranges. Results show that the highest tide will give rise to larger forces. While at lower depths, slackening of the mooring occurs. Therefore, the mooring lines must be designed to accommodate both situations.

III. NOMENCLATURE

SD	Scatter diagram
k	Given sea state
H_s	Significant wave height
Hs_0	Minimum wave height for scatter diagram
Hs_{bin}	The bin size for the scatter diagram
T_p	Peak period
Tp_0	Minimum peak period for scatter diagram
Tp_{bin}	The bin size for the scatter diagram
i,j	number of bins in the scatter diagram
JPD	Joint probability distribution
N	Number of sea states
T_z	Zero crossing period
LAT	Lowest astronomical tide
α	Scaling factor
F_1	Polynomial of the upstroke
F_2	Polynomial of the downstroke
a_n, b_n	Polynomial coefficients of up/downstroke
λ	Extension ratio
E	Standard deviation
CoG	Centre of gravity
S(ω)	Frequency dependent spectrum
ω	frequency
WEC	Wave energy converter
CSA	Cross sectional area
X_0	Original length of mooring line
ΔX	Extension of the mooring line

IV. INTRODUCTION

Tidal range impact on moorings was investigated in this paper. The device that was chosen to complete this analysis was the reference point absorber from Sandia National Laboratories. It is known as Reference Model 3 (RM3), a wave power buoy which was designed for a reference site located off the shore of Eureka in Humboldt County, California [1]. For the case of Galway bay, the device was scaled at ¼ scale of the real application to match wave conditions in the test site. To do this, Froude's scaling laws were applied [2].

The wave characteristics of Galway bay were used to complete a wave scatter diagram of the area. This data was sourced from the Marine Institute [3]. Critical extreme wave conditions were modelled which would give rise to the highest mooring forces. These corresponded to large significant wave heights and small periods. Tidal range data was also available for the Galway bay area and the maximum and minimum heights were used to determine the maximum tidal range.

ANSYS AQWA was used to simulate the device using the wave and tidal range conditions as discussed above. AQWA uses Boundary Element Method (BEM) to calculate the pressures and forces on the device and can also conduct time domain simulation with mooring lines attached. This can be used to calculate the tensions on the mooring lines under the action of extreme waves.

Two mooring configurations were used to compare the tensions on the line. Catenary lines mainly use the weight of the chain to restore the body to its original position[4]. Taut lines primarily use the elastic properties of the line as the restoring force [4]. Results showed the highest tide would give rise to larger forces. While at the lower depths, slackening of the mooring line occurred.

S Murphy, MA Bhinder, P Casaubieilh, W Sheng, Effects of Tidal Range on Mooring Systems of Wave Energy Converters,
Proceedings of the 11th European Wave and Tidal Energy Conference 6-11th Sept 2015, Nantes, France.

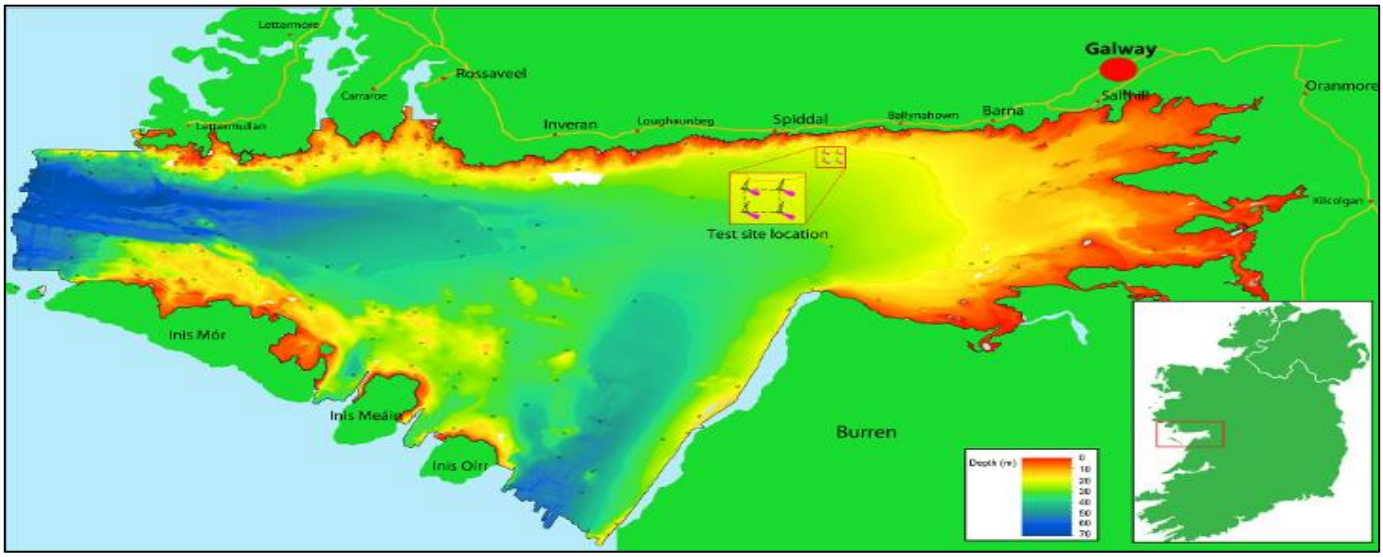

Fig. 1: Location of the wave energy test facility in Galway Bay

V. GALWAY BAY

A. *INTRODUCTION AND HISTORY*

A wave energy device test facility has been in operation in Galway bay since 2006. The specific location of the device in the bay is shown in Figure 1[5]. This test site is ideal for quarter scale testing as the waves in the bay represent quarter of the scale of the North Atlantic Ocean. Devices tested here include the OE buoy- a floating oscillating water column shown in Figure 2 and the Wavebob- a wave point absorber (Figure 3).

Fig 2: OE Buoy has been tested in Galway Bay[6]

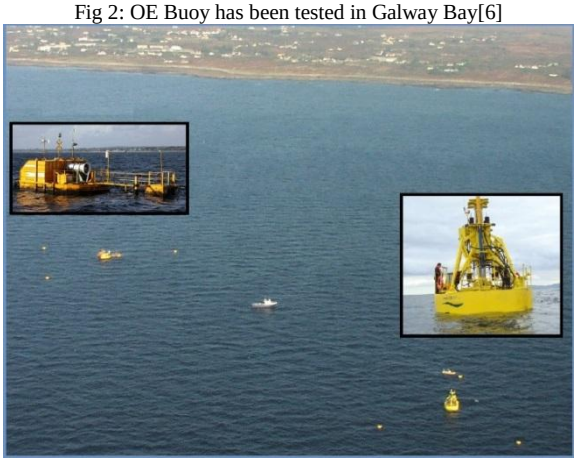

Fig 3: OE Buoy and Wavebob testing at Galway bay[7]

B. *WAVE DATA*

Wave data for the Galway bay area has been sourced from the Marine Institute data portal[3]. The following equations were used to calculate the wave scatter diagram[8].

$$SD = \sum_{k=1}^{N} \left\langle \begin{matrix} Hs_0+(i-1)Hs_{bin} \le Hs_k < Hs_0+iHs_{bin} \\ Tp_0+(j-1)Tp_{bin} \le Tp_k < Tp_0+jHTp_{bin} \end{matrix} \right\rangle \quad (1)$$

$$JPD = \frac{\sum_{k=1}^{N} \left\langle \begin{matrix} Hs_0+(i-1)Hs_{bin} \le Hs_k < Hs_0+iHs_{bin} \\ Tp_0+(j-1)Tp_{bin} \le Tp_k < Tp_0+jHTp_{bin} \end{matrix} \right\rangle}{N} \quad (2)$$

Equation 1 describes how each sea state (H_s T_p) will be categorised into particular bins in the scatter diagram (SD). Equation 2 is the joint probability distribution (JPD) equation which highlights what are the most important sea states for a given scatter diagram. The scatter diagram is shown in Figure 5 for the year 2014. From this, four states of particular interest were selected for analysis in this paper. These are shown in Table I. For this analysis, sea states on the extreme envelope of the scatter diagram will be investigated. In particular, sea states with a large significant wave height and a small period are of particular interest for moorings. Unlike large period waves, the moorings may not react well to these waves [8].

TABLE I: IRREGULAR EXTREME CONDITIONS USED in this ANALYSIS BASED on the WAVE SCATTER DIAGRAM

Wave State	Hs (m)	Tp(s)	Tz(s)	Reason
1	0.75	3.5	2.49	Highest Occurrence
2	2.75	7	4.98	Large height small period
3	4.25	9	6.41	Large height small period
4	4.25	10	7.12	Large height small period

For Table I, the relationship between T_p and T_z was taken as

$$T_p = 1.4049 T_z \qquad (3)$$

This is from the Pierson-Moskowitz spectrum for waves [9].

C. TIDAL RANGE DATA

Tidal range data was available for a number of years 2007-2010 from the Inishmore tidal gauge which obtains data every 6 minutes [10]. This data is presented in Figure 4.

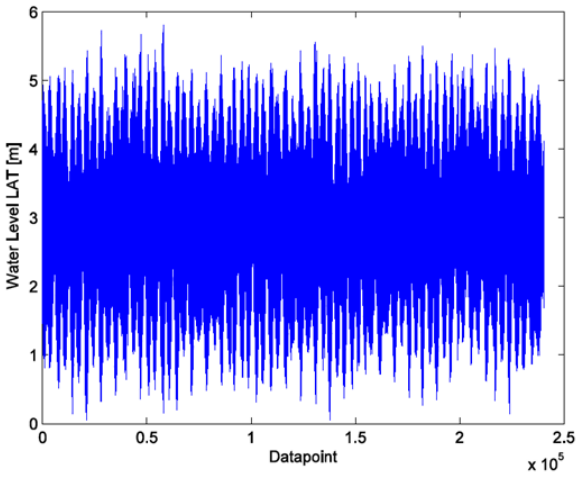

Fig. 4: Tidal Range Data for Inishmore from 2007-2010

The maximum tidal range from the above graph is 5.75 metres. In the simulation, the average, maximum and minimum tidal ranges will be investigated. The reference depth of water is the average water depth of 21.5 m in the Galway Bay test site[11].

TABLE II: TIDAL RANGES in SIMULATIONS

Level	Depth (m)
Highest Depth	24.375
Average Depth	21.500
Lowest Depth	18.625

D. WIND DATA

The wind data was sourced from the Marine Institute for January 2015. A wind scatter diagram was calculated in the same manner as the wave before (Eq.1-2). This can be represented as a wind rose diagram as well, as is shown in the following figure (Figure 6) calculated using MATLAB.

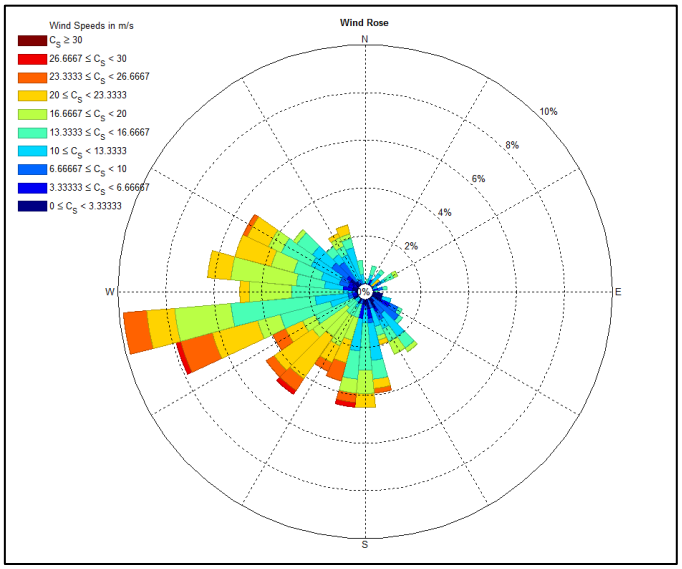

Fig. 6: Wind rose diagram for Galway bay

It is evident to see that the prevailing wind comes from the south-west as is the case in Ireland and especially the west coast[12]. Wind will not be used in the simulations.

VI. DEVICE DESCRIPTION

The device as previously mentioned is the RM3 device and it is reduced to ¼ scale using Froude scaling table as shown in Table III[13].

TABLE III: FROUDE'S SCALING LAWS

Parameter	Unit	Scaling coeff
Length	m	α
Area	m^2	α^2
Volume	m^3	α^3
Mass	kg	α^3
Force	N	α^3
Torque	Nm	α^4
Power	W	$\alpha^{3.5}$
Time	s	$\alpha^{0.5}$
Velocity	m/s	$\alpha^{0.5}$
Angular speed	rad/s	$\alpha^{-0.5}$
Unit weight of mooring line	Kg/m	α^2
Stiffness	N/m	α^2

The RM3 is based on the point absorber wave energy device. A description of the RM3 is shown in Figure 7. The float at the top of the device moves relative to spar and this relative motion is the source of the power. The power-take-off

Sig Wave Height																							
4.5-5 m	0.00	0.00	0.00	0.00	0.00	0.00	0.00	0.00	0.00	0.00	0.01	0.00	0.00	0.00	0.00	0.00	0.00	0.00	0.00	0.00	0.00	0.00	0.00
4-4.5 m	0.00	0.00	0.00	0.00	0.00	0.01	0.04	0.00	0.02	0.00	0.00	0.00	0.00	0.00	0.00	0.00	0.00	0.00	0.00	0.00	0.00	0.00	0.00
3.5-4 m	0.00	0.00	0.00	0.00	0.00	0.01	0.04	0.03	0.01	0.00	0.00	0.00	0.00	0.00	0.00	0.00	0.00	0.00	0.00	0.00	0.00	0.00	0.00
3-3.5 m	0.00	0.00	0.00	0.00	0.00	0.09	0.05	0.02	0.04	0.00	0.00	0.00	0.00	0.00	0.00	0.00	0.00	0.00	0.00	0.00	0.00	0.00	0.00
2.5-3 m	0.00	0.00	0.00	0.00	0.04	0.42	0.33	0.19	0.09	0.02	0.00	0.00	0.00	0.00	0.00	0.00	0.00	0.00	0.00	0.00	0.00	0.00	0.00
2-2.5 m	0.00	0.00	0.00	0.15	0.92	0.80	0.53	0.19	0.08	0.03	0.04	0.00	0.00	0.00	0.02	0.02	0.00	0.00	0.00	0.00	0.00	0.00	0.02
1.5-2 m	0.00	0.00	0.11	1.55	2.61	1.12	0.84	0.45	0.27	0.11	0.11	0.02	0.01	0.00	0.01	0.03	0.00	0.04	0.00	0.00	0.00	0.00	0.00
1-1.5 m	0.00	0.01	1.83	5.13	1.62	1.79	2.83	1.73	1.84	0.45	0.50	0.10	0.07	0.14	0.25	0.19	0.00	0.15	0.05	0.00	0.00	0.00	0.00
0.5-1 m	0.00	2.18	6.61	1.59	1.84	4.00	5.73	2.82	5.08	1.16	1.54	0.87	0.75	0.84	0.90	0.27	0.00	0.04	0.01	0.00	0.00	0.00	0.00
0-0.5 m	2.83	4.98	0.61	0.57	1.38	3.02	5.44	2.81	5.20	1.46	2.24	0.77	0.70	0.60	0.45	0.29	0.00	0.21	0.05	0.00	0.00	0.00	0.00
Peak Period	1-2 s	2-3 s	3-4 s	4-5 s	5-6 s	6-7 s	7-8 s	8-9 s	9-10 s	10-11 s	11-12 s	12-13 s	13-14 s	14-15 s	15-16 s	16-17 s	17-18 s	18-19 s	19-20 s	20-21 s	21-22 s	22-23 s	

Fig. 5: Wave scatter diagram for the Galway Bay area. Area of interest marked with blue circle above.

(PTO) system is a hydraulic system[14].

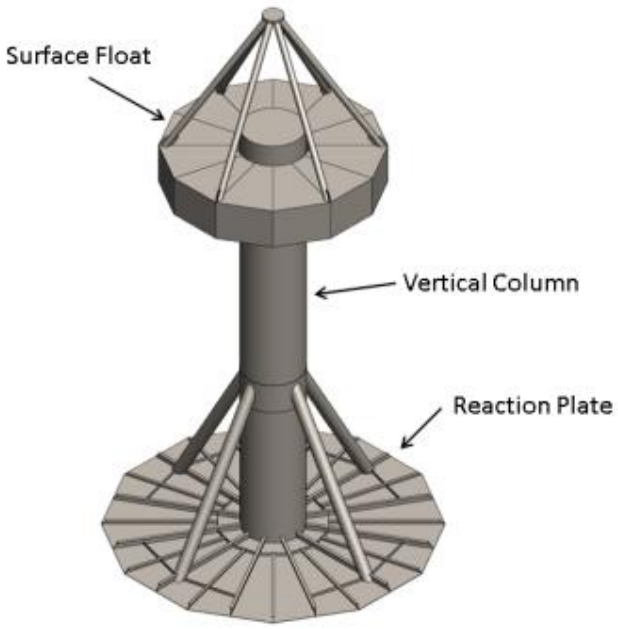

Fig. 7: Sandia open Source RM3 device[15]

For the simulation, the RM3 will be treated as one body as tension on the mooring lines is only investigated. The power-take-off (PTO) is not considered. The device geometry was created in ANSYS AQWA Design Modeller software based on the specific geometry of the RM3 device at ¼ scale according to Table III. The body was meshed using AQWA Hydrodynamic Diffraction suite as shown in Figure 8.

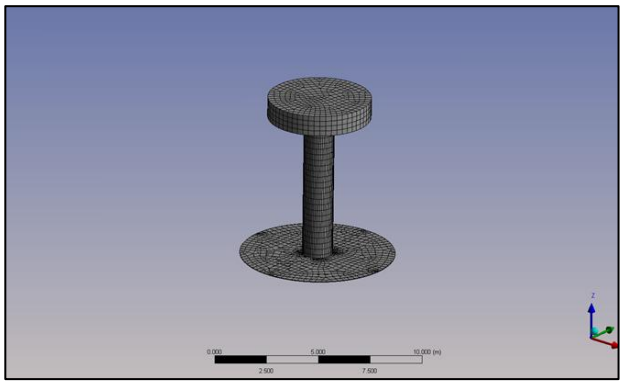

Fig. 8: Mesh of the RM3 device in ANSYS AQWA

VII. MOORING PROPERTIES

A. *CATENARY PROPERTIES*

A catenary chain is used to moor the device to the seabed. The connection points on the device are shown in Table IV. The anchor points on the seabed are shown in Table V. The system is designed for the average water depth of 21.5 m.

TABLE IV: CONNECTION POINTS on RM3 MODEL

Line	X	Y	Z
1	0.73375	0	-2.795
2	-0.367	0.6355	-2.795
3	-0.367	-0.6355	-2.795

TABLE V: ANCHOR POINTS for the MODEL SET-UP and LINE LENGTHS.

Line	X	Y	Z	Length(m)
1	93.25	0	-21.5	96.75
2	-46.625	80.757	-21.5	96.75
3	-46.625	-80.757	-21.5	96.75

Froude's similarities were used to scale down the mooring line for this application. The key property that was scaled down was the mass/unit length using α^2 (Table III).

TABLE VI: CATENARY PROPERTIES for AQWA

Property	Value	Units
Mass/Length	11.1	kg/m
Nominal Diameter	0.022	m[16]
Effective Diameter	0.04158	m[17]
Effective CSA	0.001358	m^2
Axial Stiffness(EA)	48,884,000	N[18]

B. *TAUT PROPERTIES*

The taut set-up incorporates an elastic component as the mooring line. This elastic component will be based on the Seaflex® mooring material (Figure 9). Seaflex® is an elastic mooring product made of a reinforced homogeneous rubber hawser.[19]

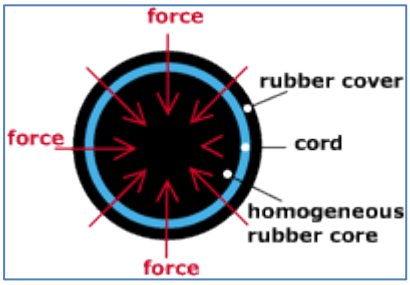

Fig. 9: Seaflex® component

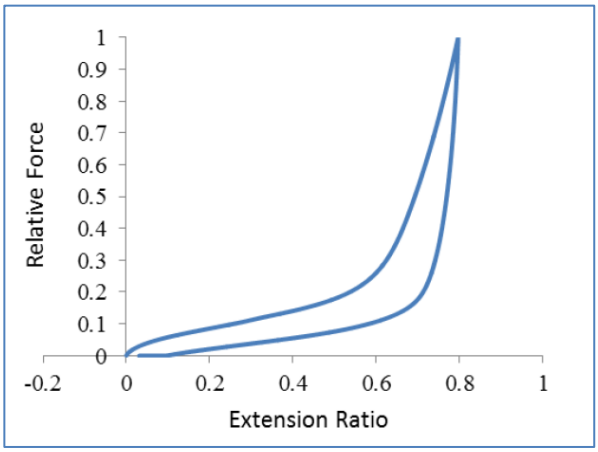

Fig 10: Hysteresis load-strain loop of Seaflex® component[2]

Figure 10 shows the experimental data of upstroke and downstroke of the force versus extension ratio of the Seaflex® component normalised.

In modelling the Seaflex® component, especially its nonlinear hysteresis loop in the stretching and de-stretching process, two polynomial functions have to be used to represent the upstroke strain-stress curve and down-stroke strain-stress curve. For example, for up-stroke (stretching), the curve can be represented by a polynomial function F_1 as

$$F_1 = \sum_{n=1}^{M} a_n \lambda^n \qquad (4)$$

The corresponding spring coefficient (extension ratio dependent) is

$$\frac{dF_1}{d\lambda} = \sum_{n=1}^{M} n a_n \lambda^{n-1} \qquad (5)$$

for down-stroke ('de-stretching'), the curve can be represented by a polynomial function F_2 as

$$F_2 = \sum_{n=1}^{M} b_n \lambda^n \qquad (6)$$

The corresponding spring coefficient (extension ratio dependent) is

$$\frac{dF_2}{d\lambda} = \sum_{n=1}^{M} n b_n \lambda^{n-1} \qquad (7)$$

For coefficients a_n and b_n, a least square method can be used to get the best fit coefficients for the up-stroke and down-stroke curves.

For up-stroke, the error between the fit function and the measured data is calculated as

$$E = \sum_{i=1}^{N} \left(F_i^e - \sum_{n=1}^{M} a_n \lambda^n \right)^2 \qquad (8)$$

where F_i^e is the measured tension acting on the Seaflex® component.

To get the minimized error, a relation must be satisfied as

$$\frac{\partial E}{\partial a_i} = 0 \qquad (i=1, 2, \ldots, M) \qquad (9)$$

which leads to a simultaneous equation,

$$\begin{cases} a_1 \sum_{i=1}^{N} \lambda_i^2 + a_2 \sum_{i=1}^{N} \lambda_i^3 + \ldots + a_M \sum_{i=1}^{N} \lambda_i^{M+1} = \sum_{i=1}^{N} F_i^e \lambda_i \\ a_1 \sum_{i=1}^{N} \lambda_i^3 + a_2 \sum_{i=1}^{N} \lambda_i^4 + \ldots + a_M \sum_{i=1}^{N} \lambda_i^{M+2} = \sum_{i=1}^{N} F_i^e \lambda_i^2 \\ \ldots \\ a_1 \sum_{i=1}^{N} \lambda_i^{M+1} + a_2 \sum_{i=1}^{N} \lambda_i^{M+2} + \ldots + a_M \sum_{i=1}^{N} \lambda_i^{2M} = \sum_{i=1}^{N} F_i^e \lambda_i^M \end{cases} \qquad (10)$$

In solving the above simultaneous equation, we can obtain the fitting coefficients, a_n (n=1,2,..,M). A similar approach can be used for down-stroke process[20].

In AQWA, for a mooring line with non-linear stiffness, one can input a non-linear polynomial to represent the load-strain curve. This requires a 5 term polynomial of the line in question. The average of the upper and lower polynomials from Figure 10 was calculated. This is shown in figure 11 below. This line will be used to represent the taut mooring in AQWA.

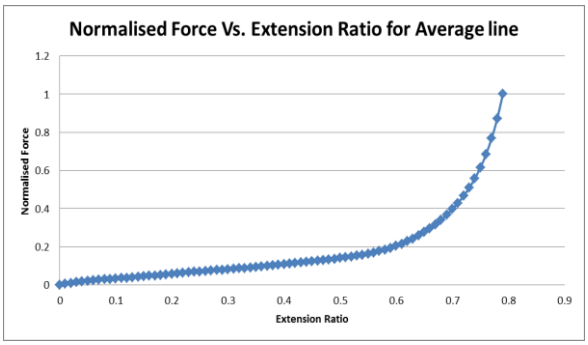

Fig.11: Average load-extension ratio of taut mooring

For the simulation, the number of components was increased and the initial extension of the line was set to 30%. This ensured the same initial tension in AQWA as the catenary both designed for the average depth of 21.5 m. For AQWA, it is required to have these coefficients in terms of *actual extension* of the line and not *extension ratio*. Using the following equation, the coefficients input into AQWA were calculated[21].

$$\frac{a_1}{X_0^1}\Delta X + \frac{a_2}{X_0^2}\Delta X^2 + \frac{a_3}{X_0^3}\Delta X^3 + \frac{a_4}{X_0^4}\Delta X^4 + \frac{a_5}{X_0^5}\Delta X^5 \quad (11)$$

VIII. SIMULATION SET-UP

AQWA is an engineering analysis suite which can simulate the effect of waves, wind and current on floating or fixed offshore structures. There are two main parts to the AQWA modelling system. The hydrodynamic diffraction section provides one with frequency dependent results of key hydrodynamic parameters such as added mass, radiation damping, Response Amplitude Operators (RAO's) and excitation forces. These frequency domain results can be then transformed as the input into the time domain suite of AQWA. In the time domain, the mooring loads can also be simulated under the action of regular waves, irregular waves, wind and current or a combination of these.

Figure 12 shows the mooring set-up for the catenary layout.

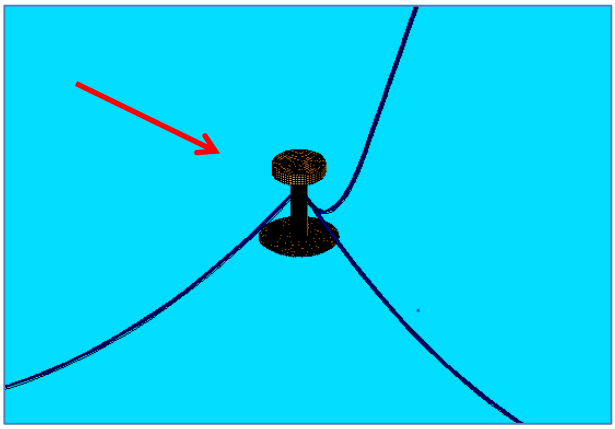

Fig. 12: RM3 meshed body in catenary mooring layout- Wave direction as shown by the arrow.

The motion was restricted to heave and surge motion only for the analysis. This was completed by using Deck 12 in the DAT (data) file of the AQWA programme. The other 4 degrees of freedom were constrained[22].

The use of an external force routine in AQWA allowed input of quadratic damping for the heave and surge motion to account for the viscous drag of the heave plate[22]. The values were scaled using α^2 and are shown in the following table. The large heave damping value represents the heave plate of the RM3 device as shown by the base of device in Figure 8.

TABLE VII: DAMPING VALUES USED for the SIMULATION SCALED USING α^2 [23]

Motion	Value	Units
Surge	7500	N/((m/s)^2)
Heave	108750	N/((m/s)^2)

The Pierson-Moskowitz spectrum was used for the irregular waves as discussed previously. If the wind blows constantly for a long period of time over a large fetch, then the waves will eventually reach a point of equilibrium with the wind. This is known as a fully developed sea[24]. The spectrum equation associated with this condition is Eq. 12 which is taken from the AQWA Theory Manual[25].

$$S(\omega) = 4\pi^3 \frac{H_S^2}{T_Z^4}\frac{1}{\omega^5}\exp\left(-\frac{16\pi^3}{T_Z^4}\frac{1}{\omega^4}\right) \quad (12)$$

The taut layout is shown in figure 13 for the modelling. It can be seen that the seabed footprint is a lot smaller for taut mooring rather than catenary. The set-up for the taut is such that each line makes an angle of 60° to the seabed.

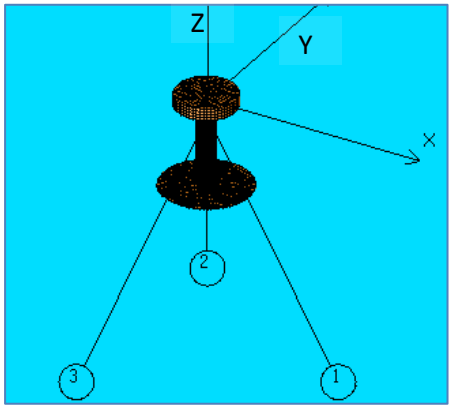

Fig.13: Taut set-up with line numbers as shown. Wave from –X direction.

IX. RESULTS

The catenary and taut moorings were simulated for 500 seconds using a time step of 0.01 seconds. Figure 14 shows the result of tension for catenary mooring under the action of Wave State 2(Table I) at the depth of 21.5 m. The results have been normalised to the largest force the mooring lines experienced. Figure 15 shows the results of the taut mooring to the same wave state. The catenary line experiences higher loads than that of the taut line.

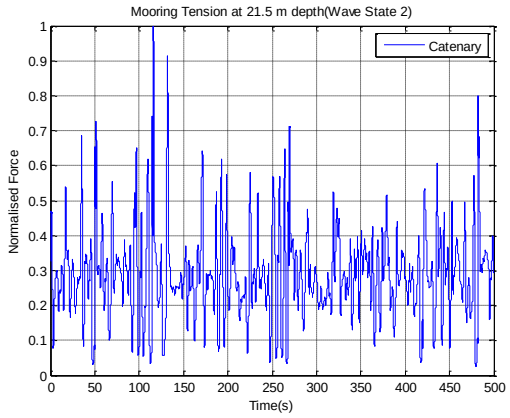

Fig. 14: Normalised catenary tension for wave state 2 at 21.5 m depth

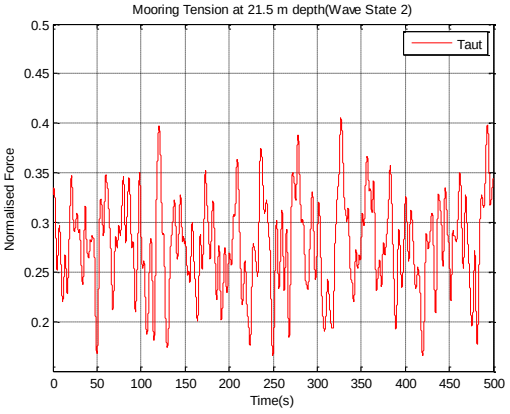

Fig.15: Normalised taut tension for wave state 2 at 21.5 m depth

Figure 16 shows the motion of the CoG of the body in heave for the catenary mooring. Figure 17 is the heave motion of the taut configuration. The motion of both is very similar due to the large damping associated with the heave motion which is to represent the heave plate of the system (see Table VII).

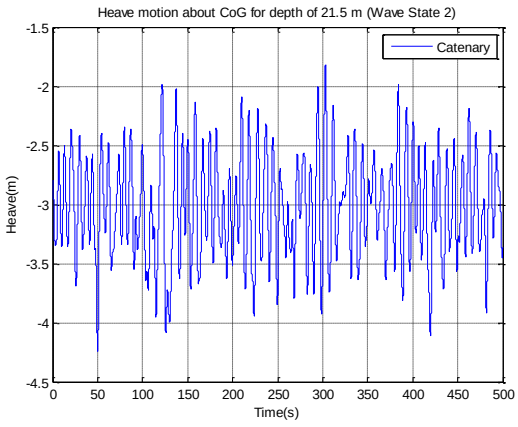

Fig.16: Heave motion for catenary mooring about CoG for depth of 21.5m for Wave State 2

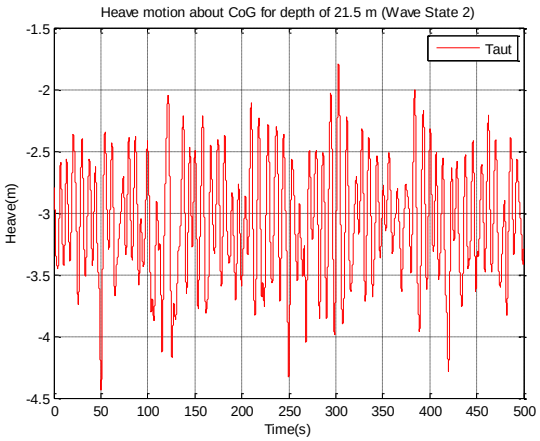

Fig.17: Heave motion for taut mooring about CoG for depth of 21.5m

Figure 18-19 shows the surge motion of the catenary chain and taut mooring for the depth of 21.5 m and Wave State 2. Taut mooring allows greater motion in surge than that of the catenary.

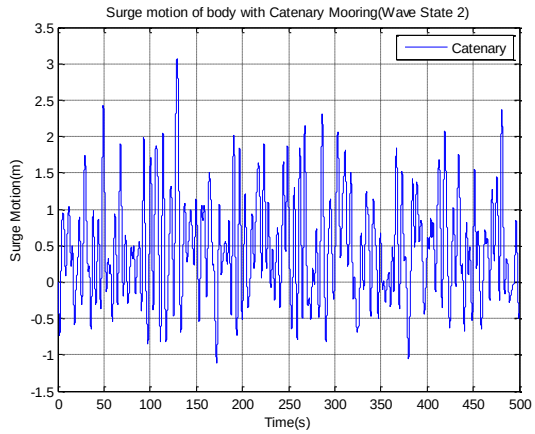

Fig. 18: Surge motion of the CoG for depth of 21.5 and catenary mooring

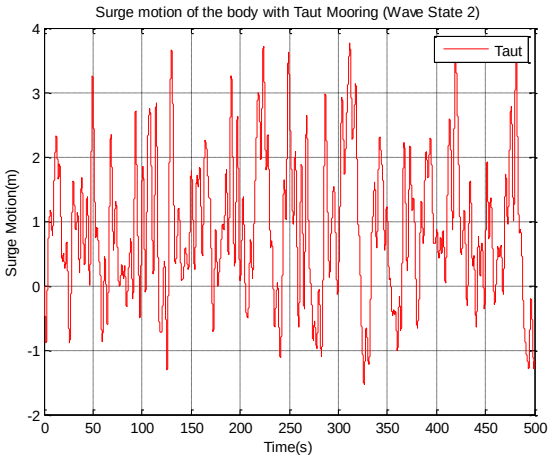

Fig. 19: Surge motion of the CoG for depth of 21.5 and taut mooring

In the following three figures (Figure 20-22), the maximum force over the time series has been tabulated for each depth and each wave state. The largest of these forces has been taken as reference and everything has been normalised to this value.

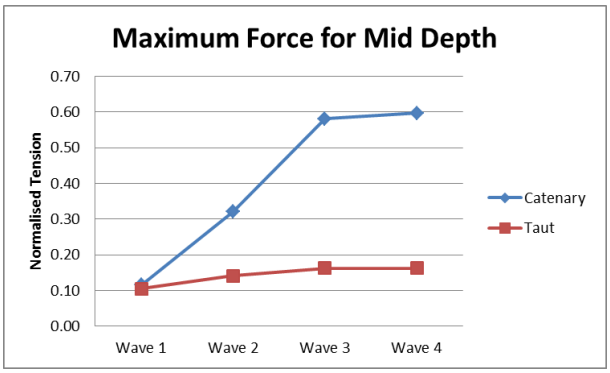

Fig. 20: Maximum force recorded for taut and catenary at mid depth

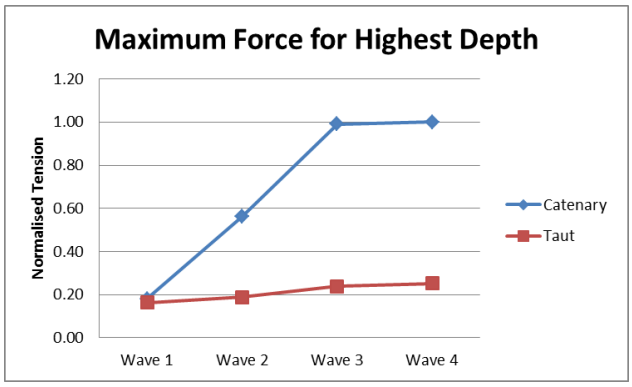

Fig. 21: Maximum force recorded for catenary and taut at highest depth

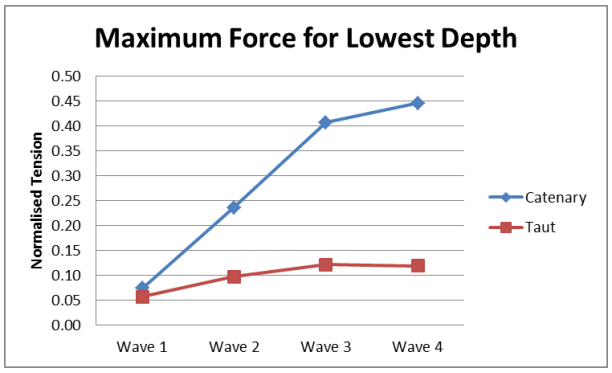

Fig. 22: Maximum force recorded for catenary and taut at lowest depth

The maximum normalised surge displacement values from the CoG of each depth and wave state are shown in Figure 23-25.

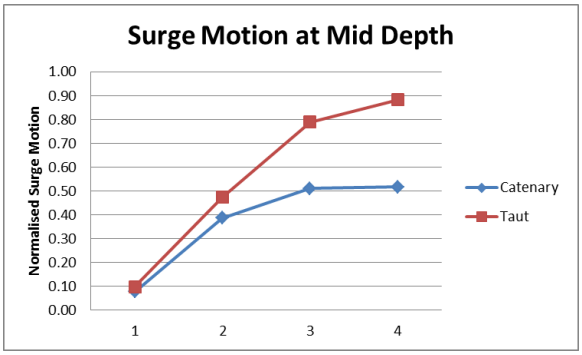

Fig. 23: Maximum surge motion from CoG at mid depth

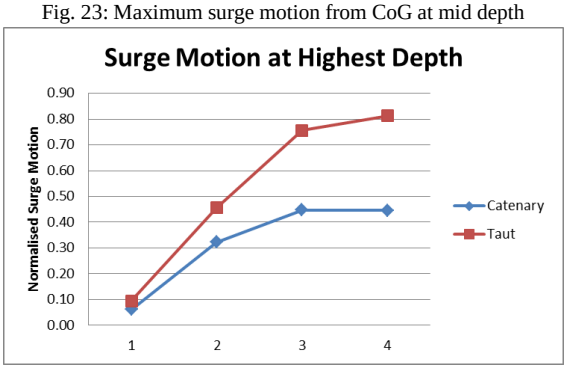

Fig. 24: Maximum surge motion from CoG at highest depth

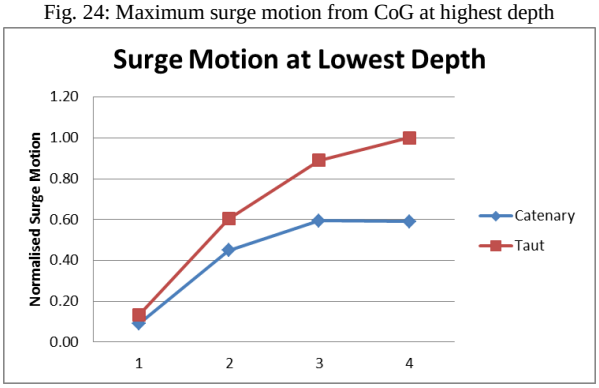

Fig.25: Maximum Surge motion from CoG at lowest depth

The surge motion for the taut configuration for wave state 3 for the varying depths is shown in Figure 26. It can be seen that at higher depths, the maximum value of surge is decreased.

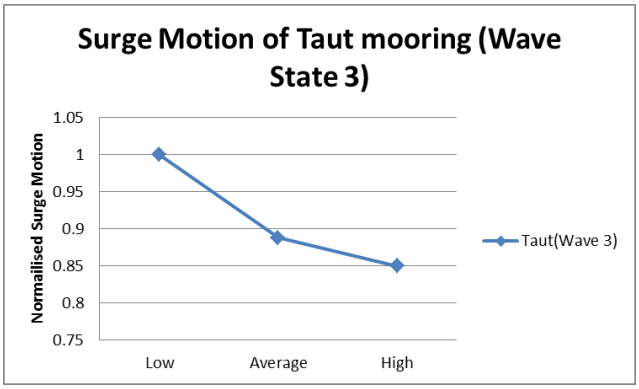

Fig. 26: Maximum surge displacement from CoG at varying depths

Results from the ANSYS simulations are shown in Table VIII to XIII.

TABLE VIII: TAUT DATA from AQWA- MID DEPTH

Taut- Average Depth			
	Tension	Max Ext	Slack Line
Wave 1	0.11	32.19%	No
Wave 2	0.14	40.85%	No
Wave 3	0.16	47.18%	No
Wave 4	0.16	47.10%	No

TABLE IX: TAUT DATA from AQWA- HIGH TIDE

Taut- Highest Depth			
	Tension	Max Ext	Slack Line
Wave 1	0.16	47.00%	No
Wave 2	0.19	54.15%	No
Wave 3	0.24	60.38%	No
Wave 4	0.25	61.34%	No

TABLE X: TAUT DATA from AQWA- LOW TIDE

Taut- Lowest Depth			
	Tension	Max Ext	Slack Line
Wave 1	0.06	18.10%	No
Wave 2	0.10	30.42%	Yes
Wave 3	0.12	35.95%	Yes
Wave 4	0.12	35.28%	Yes

TABLE XI: CATENARY DATA from AQWA- MID DEPTH

Catenary- Average Depth			
	Tension	% Break Load	Slack Line
Wave 1	0.12	3.45	No
Wave 2	0.32	9.58	No
Wave 3	0.58	17.37	Yes
Wave 4	0.60	17.85	Yes

TABLE XII: CATENARY DATA from AQWA- HIGH TIDE

Catenary- Highest Depth			
	Tension	% Break Load	Slack Line
Wave 1	0.18	5.35	No
Wave 2	0.56	16.74	Yes
Wave 3	0.99	29.84	Yes
Wave 4	1.00	29.86	Yes

TABLE XIII: CATENARY DATA from AQWA- LOW TIDE

Catenary- Lowest Depth			
	Tension	% Break Load	Slack Line
Wave 1	0.07	2.22	No
Wave 2	0.24	7.07	No
Wave 3	0.41	12.17	Yes
Wave 4	0.45	13.31	Yes

X. DISCUSSION

From the layout in AQWA, the catenary mooring required a greater length of chain and footprint when compared to the taut configuration. This may need to be considered in the designing of the mooring system. As a result, the watch circle of the catenary mooring is significantly larger than that of the taut mooring. This could be an important factor when considering arrays[26]. The taut mooring will have a smaller impact to the seabed around it compared to the catenary mooring which will affect the local environment and erode the seabed. The catenary mooring will have only horizontal loads at the anchor point while the taut mooring will have horizontal and vertical loads on the anchor and require a more sophisticated vertically loaded anchor(VLA)[26, 27].

The heave displacement for both mooring set-ups is very similar. This is due to the presence of the damping which represents the large heave plate at the base of the model. This is shown in Figures 16-17.The displacement in surge is greater for the taut set-up rather than that of the catenary set-up. This is shown in the Figures 18-19 and the Figures 23-25. Further design of the taut mooring would be required to increase the stiffness. An interesting result is the fact that as the depth increased, the lower the surge motion of the device with both mooring configurations. This is due to the fact that there would be more pretension on the line in the deeper waters. This can be seen for taut mooring in Figure 26.

The forces recorded from the ANSYS AQWA simulations are higher for the catenary moorings rather than the taut configuration. This is shown in Figures 14-15 and in the Figures 20-22. The force on the mooring lines also increases with increasing depth. The forces on the catenary moorings reached a maximum of 29% of the breaking load. Even considering a factor of safety of 2, the forces on the moorings would not have exceeded this value, however, it is noted that only heave and surge motions has been analysed in this paper. The extension of the taut mooring line reaches a maximum of 61% which is less than the experimental limit of 70%. More mooring lines in parallel could be considered to increase the stiffness. However, increasing the stiffness will also increase the force on the line so an iterative process would be required.

Slack line was observed in the catenary chain for all depths excluding the highest occurrence wave. This leads to shock

loading of the chain and results in large spikes in the force which could damage the mooring. The taut mooring needs to be designed to stay under tension at all times. This is not the case in the simulations run at the lowest depth, so further design iterations would be required. The taut mooring would be designed in such a way as to be under tension at all times similar to the results for the largest and mid depth in Table VIII and IX.

XI. CONCLUSION

Mooring of a wave energy converter at three different depths has been considered to determine the impact the change in depth has on the moorings. The device that was chosen to complete this analysis was the device known as Reference Model 3(RM3) - a point absorber. Galway bay test site was chosen as the location in this modelling. The body has been moored with both catenary and taut configurations. ANSYS AQWA was used to simulate the device using the wave conditions and tidal range of Galway bay in heave and surge motion.

From the simulation, it was found that the catenary mooring results in higher forces on the line compared to the taut moorings at all depths. The forces on the mooring lines increase with increased depth. The taut mooring allowed greater surge motion of the device. The higher the depth/greater pretension, the smaller the surge motion will be. The heave for both mooring configurations was similar due to presence of the heave plate. Slackness of the catenary chain is an issue noted in the simulations with larges forces on the moorings immediately upon loading after slack chain occurs. The taut mooring also goes slack at the lowest depth and further design would be required to maintain tension on the line at all times. Tidal range may be a critically important parameter to consider when designing mooring systems for WECs. The system needs to be able to cope with the water depth changes due to high or low tides and to avoid the very large loads or slack loads on mooring lines.

ACKNOWLEDGEMENTS

The authors would like to acknowledge the data sourced from the Marine Institute online data portal. The author would also like to acknowledge the Marine Renewable Energy Ireland (MaREI).

REFERENCES

[1] V. S. Neary, M. Lawsom, M. Previsic, A. Copping, K. C. Hallett, A. Labonte, *et al.*, "Methodology for design and economic analysis of Marine Energy Conversion (MEC) technologies," 2014.

[2] P. Casaubieilh, F. Thiebaut, B. Bosma, C. Retzler, M. Shaw, Y. Letertre, *et al.*, "Performance Improvements of Mooring Systems for Wave Energy Converters," presented at the Renew 2014 -1st International Conference on Renewable Energies Offshore, Lisbon, Portugal, 2014.

[3] Marine Institute *Wave Data for Galway Bay*. Available: http://data.marine.ie/

[4] R. E. Harris, L. Johanning, and J. Wolfram, "Mooring systems for wave energy converters: A review of design issues and choices," *Marec2004*, 2004.

[5] Sustainable Energy Authority of Ireland (SEAI). *Location map for Galway Bay 1/4 scale test site*. Available: http://www.seai.ie/Renewables/Ocean_Energy/Galway_Bay_Test_Site/Map_of_test_site.html

[6] Ocean Energy. *OceanEnergy agree to install the first device at the Wave Hub off Cornwall Coast*. Available: http://oceanenergy.ie/news/

[7] Sustainable Energy Authority of Ireland (SEAI). *Galway Bay Test Site*. Available: http://www.seai.ie/Renewables/Ocean_Energy/Galway_Bay_Test_Site/

[8] V. Harnois, L. Johanning, and P. R. Thies, "Wave Conditions Inducing Extreme Mooring Loads on a Dynamically Responding Moored Structure," in *10th European Wave and Tidal Energy Conference,(University of Aalborg, Denmark, September 2013)*.

[9] D. N. Veritas, "DNV-RP-H103 Modelling and Analysis of Marine Operations," ed: APRIL, 2011.

[10] Marine Institute. *Irish National Tide Gauge Network Real Time Data* Available: http://data.marine.ie/Dataset/Details/20932

[11] SmartbayIreland. *Galway Bay 1/4 Scale Ocean Energy Test Site*. Available: http://www.smartbay.ie/Facilities/GalwayBayOceanEnergyTestSite.aspx

[12] Met Eireann. *Wind Over Ireland*. Available: http://www.met.ie/climate-ireland/wind.asp

[13] D. Vassalos, "Physical modelling and similitude of marine structures," *Ocean engineering*, vol. 26, pp. 111-123, 1998.

[14] Ocean Power Technologies Website Available: http://www.oceanpowertechnologies.com/

[15] V. S. Neary, M. Previsic, R. A. Jepsen, M. J. Lawson, Y.-H. Yu, A. E. Copping, *et al.*, "Methodology for Design and Economic Analysis of Marine Energy Conversion(MEC) Technologies," Sandia National Laboratories, Albuquerque, New Mexico March 2014.

[16] Saxton Marine. *Chain and Kenter Shackle Weights*. Available: http://www.saxtonmarine.co.uk/kenter_shackle_chain_weights.html

[17] OrcaFlex Documentation. *Chain: Outer, Inner and Contact Diameter*. Available: http://www.orcina.com/SoftwareProducts/OrcaFlex/Documentation/Help/Content/html/Chain,Outer,InnerandContactDiameter.htm

[18] OrcaFlex Documentation. *Chain: Axial and Bending Stiffness*. Available: http://www.orcina.com/SoftwareProducts/OrcaFlex/Documentation/Help/Content/html/Chain,AxialandBendingStiffness.htm

[19] SEAFLEX. *SEAFLEX Mooring System*. Available: http://www.seaflex.net/index.php?option=com_content&view=article&id=27:seaflex-mooring-system&catid=23&Itemid=10

[20] W. Sheng and M. A. Bhinder, "D2.3 Mooring Analysis Report," University College Cork, Ireland, Geowave FP7 European Project 2014.

[21] ANSYS, *ANSYS AQWA User's Manual v15.0*, 2013.

[22] ANSYS, *ANSYS AQWA Reference Manual v15.0* 2013.

[23] M. A. Bhinder, M. Karimirad, S. Weller, Y. Debruyne, M. Gurinel, and W. Sheng, "Modelling mooring line non-linearities(material and geometric effects) for a wave energy converter using AQWA,SIMA and Orcaflex," submitted in Proc. of EWTEC, Nantes, 2015.

[24] J. Journée and W. Massie, *Offshore hydromechanics*: TU Delft, 2000.

[25] ANSYS, *ANSYS AQWA Theory Manual v15.0* 2013.

[26] J. Fitzgerald and L. Bergdahl, "Considering mooring cables for offshore wave energy converters," in *Proc 7th European Wave Tidal Energy Conf, Porto, Portugal*, 2007.

[27] J. Colliat, "Anchors for deepwater to ultradeepwater moorings," in *Proceedings of the 34th Annual Offshore Technology Conference (OTC'02)*, 2002, pp. 2695-2703.